arXiv:1404.1862v1 [cond-mat.str-el] 7 Apr 2014

How chromium doping affects the correlated electronic structure of V_2O_3

Daniel Grieger[1] and Frank Lechermann[2]

[1] *SISSA, Via Bonomea 265, I-34136 Trieste, Italy*

[2] *I. Institut für Theoretische Physik, Universität Hamburg, Jungiusstr. 9, D-20355 Hamburg, Germany*

(Dated: April 8, 2014)

The archetypical strongly correlated Mott-phenomena compound V_2O_3 is known to show a paramagnetic metal-insulator transition driven by doping with chromium atoms and/or (negative) pressure. Via charge self-consistent density-functional theory+dynamical mean-field theory calculations we demonstrate that these two routes cannot be understood as equivalent. To this end, the explicit description of Cr-doped V_2O_3 by means of supercell calculations and the virtual crystal approximation is performed. Already the sole introduction of chromium's additional electron to the system is shown to modify the overall correlated electronic structure substantially. Correlation-induced charge transfers between Cr and the remaining V ions occur and the transition-metal orbital polarization is increased by the electron doping, in close agreement with experimental findings.

PACS numbers: 71.30.+h, 71.15.Mb, 71.10.Fd

I. INTRODUCTION

The vanadium sesquioxide V_2O_3 is among the most prominent strongly correlated compounds and has already been studied in many theoretical works.[1–11] The three major phases found in its prototype phase diagram[12,13] at temperature T are a paramagnetic metal (PM) and a paramagnetic insulator (PI) based on the corundum crystal structure as well as a monoclinic antiferromagnetic insulating phase at lower T. Note that this picture might not even be complete, as the discovery of new more exotic phases such as paramagnetic monoclinic[14] or spin density wave[15] structres suggests.

At ambient T and pressure p, the stoichiometric compound is in the metallic state. Along the crystallographic c-axis of the corundum structure V-V pairs appear and a honeycomb lattice marks the ab-plane. The V ions reside within an octahedron of O ions, which in the present case build up a trigonal crystal field around the transition metal. The low-energy t_{2g} orbitals of the V($3d$) shell are split into an a_{1g} and two degenerate e'_g orbitals. Formally the vanadium ion has the $3d^2$ valence configuration, i.e. is in the V^{3+} oxidation state.

In experiment the traditional phase changes at constant temperature are realized through doping the material either with Cr or Ti. While chromium doping allows for the metal-to-insulator transition (MIT), Ti-doping is more relevant to map out phase regions at rather high/low temperature. Since the readily measurable structural effect of adding Cr lies in some lattice expansion,[12,13] the role of Cr-doping in literature is often fully reduced to the picture of applying negative p, therewith rendering the V_2O_3 MIT to a realistic example of Mott's original thinking about electron localization. However substitutional Cr is not isovalent with V, but has one additional electron in the valence. Yet the details of this specific electron doping as well as the resulting Cr-induced electronic-structure effects have so far not really been studied on an elaborate level. In other words, the explicit defect-related physics of Cr-doping in V_2O_3 may bear much more processes relevant for the driving forces behind the Mott transition than pure structural effects. In this regard the elder orbital-polarization measurements of Park *et al.*[16] are especially interesting. They revealed a a much larger vanadium e'_g/a_{1g} orbital polarization in the (Cr-doped) PI than in the metallic phase. Recenty Rodolakis *et al.*[17,18] compared the Cr doping-driven MIT with a truly pressure-driven MIT, i.e. by increasing pressure on insulating $(V_{0.92}Cr_{0.08})_2O_3$. It was observed that in the latter case the (e'_g, a_{1g}) orbital occupations hardly vary across the MIT. Hence the enhanced orbital polarization in the PI appears to be bound to the explicit doping-driven character of the MIT realization. This observation is confirmed by recent calculations based on the charge self-consistent combination of density functional theory (DFT) with dynamical mean-field theory (DMFT), the so-called DFT+DMFT approach.[9] There lattice-expanded stoichiometric V_2O_3 became Mott-insulating, but indeed without a strong change in the e'_g/a_{1g} orbital polarization.

In this work we explicitly show that the Cr doping of V_2O_3 can be understood as a key constituent of the increased e'_g/a_{1g} orbital polarization. Charge self-consistent DFT+DMFT applied to substitutional defect supercells as well as in the virtual crystal approximation (VCA) reveal that the additional valence electron of chromium is not a passive spectator only giving rise to a change in total volume. Instead it plays and active part in the correlated electronic structure and supposingly appears as a vital ingredient in the mechanisms underlying the V_2O_3 MIT.

II. THEORETICAL FRAMEWORK

Our first-principles DFT+DMFT approach[9] is based on a mixed-basis pseudopotential (MBPP) technique[19] for the DFT part and a hybridization-expansion continous-time quantum Monte-Carlo impu-

rity scheme[20,21] to solve the DMFT impurity problems posed by the realistic materials problem. The local density approximation (LDA) to DFT is utilized, crosschecks with the generalized-gradient approximation (GGA) do not lead to relevant modifications of the results. Throughout the work we rely on correlated subspaces composed of the projected (e'_g, a_{1g}) orbital[22–24] threefolds from the Kohn-Sham bands with dominant transition-metal $3d$ weight. Thus at each charge self-consistent convergence step a multi-orbital Hubbard Hamiltonian employing the complete rotational invariant Coulomb interactions is applied at each correlated site taking part in the overall correlated subspace. For the parametrization of the Coulomb integrals we choose a Slater-Kanamori form with Hubbard U=5 eV and and Hund's exchange $J_{\rm H}$=0.93 eV for both Cr and V orbitals, as already utilized in earlier simplified LDA+DMFT studies for V_2O_3.[6]

Cr doping of vanadium sesquioxide is computationally realized in two ways. First via the replacement of a single vanadium atom by a chromium atom in the original four-V-site unit cell as well as in an eight-V-site supercell. Accordingly, this amounts to a doping level of x=0.25 and x=0.125, in our chosen $V_{2(1-x)}Cr_{2x}O_2$ notation, respectively. Albeit larger than in most experiments, these scenarios are geared to corrobate the key qualitative doping effects. Second we compared this direct approach to a treatment within VCA, allowing for in principle arbitrary doping levels in an averaged-medium picturing of the problem. There the V pseudopotential is replaced by an effective pseudopotential with nuclear charge $\tilde{n_c}=x\,n_c^{\rm Cr}+(1-x)\,n_c^{\rm V}$, with $n_c^{\rm Cr}$, $n_c^{\rm V}$ as the Cr, V nuclear charges. Note however that explicit self-energy effects due to disorder, i.e. finite lifetimes due to a given disorder strength, are not included in the VCA approach. However it is believed that such direct effects of disorder are to a good approximation negligible compared to the dominant impact of Coulomb correlations in V_2O_3.

In order to include the effect of local structural relaxations due to Cr doping, the Wyckoff positions of the atomic sites are optimized within LDA for all structures used in this work. The lattice parameters have been fixed at their values of stoichiometric V_2O_3 at ambient pressure in the metallic phase, as found in Ref. 25. Possible effects of the enlargement of the unit cell have been published previously in Ref. 9. The $\frac{c}{a}$ ratio of the hexagonal lattice parameters, which changes in a nontrivial way at the metal-insulator transition,[25] may be expected to have a significant influence on the electronic structure and is thus investigated explicitly in section IV B.

III. LDA PERSPECTIVE OF CR-DOPED V_2O_3

Before tackling the effects of strong electronic correlations in a realistic many-body scope, it is useful to take a closer look at how Cr doping affects the plain LDA electronic structure. The results concerning the spectral properties are summarized in Fig. 1. For undoped V_2O_3, the Kohn-Sham (KS) band structure shows the well-known transition-metal-oxide splitting into completely filled oxygen-like bands (from about -8 eV to -4 eV) and partially filled vanadium $3d$-like bands (around the Fermi energy $\varepsilon_{\rm F}$). The latter show the above-mentioned ligand-field splitting into a partially filled t_{2g} and an empty e_g manifold. The structural relaxation within LDA leads to a less pronounced gap between these two compared to previous work using experimental values for the Wyckoff positions.[2,9] The addition of one electron via one Cr impurity atom does not lead to significant changes of the KS density of states (DOS), apart from a seemingly small overall generic shift in energy. The trigonal crystal-field splitting of the t_{2g} manifold into two e'_g and one a_{1g} state is also qualitatively very similar for all doping levels. Especially the a_{1g} state keeps its pronounced bonding-antibonding structure caused by the relatively large hopping in the crystallographic c direction. Note further that in the doped supercell calculations (with more than four V/Cr atoms), the e'_g states are formally nondegenerate. Descriptively speaking, they can be distingiushed whether or not they point towards a Cr atom. The respective occupation values are averaged in the following, if necessary.

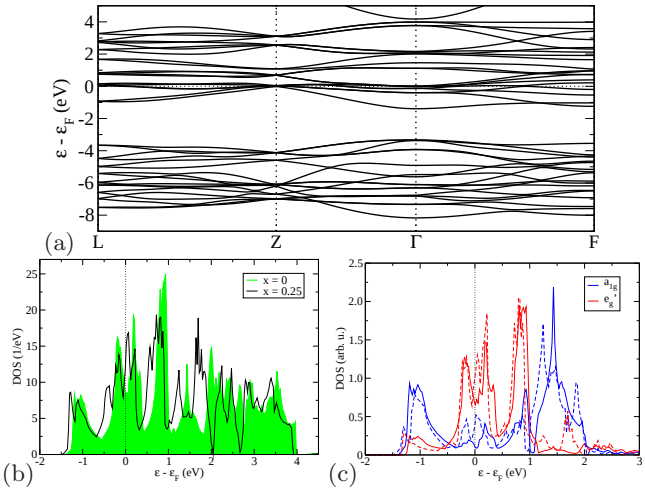

FIG. 1. (Color online) LDA spectral data. (a) Band structure of undoped V_2O_3 along high symmetry lines. (b) Total density of states (DOS) of the doped supercell calculations for different values of Cr doping. (c) Partial DOS projected onto the a_{1g} and e'_g basis orbitals of one vanadium atom.

Fig. 2 displays the LDA-derived KS band structure near the Fermi energy with and without doping together with the k-resolved respective a_{1g}, e'_g weight on each band (via so-called "fatbands"). The latter again reflect the a_{1g} bonding/antibonding character and the more localized e'_g behavior associated with narrower bands near the Fermi level. Notably however, small a_{1g} spectral-weight contribution can also be found near $\varepsilon_{\rm F}$. In the undoped case the Z point in the first Brillouin zone (BZ) marks close to the Fermi level a manifold band-crossing

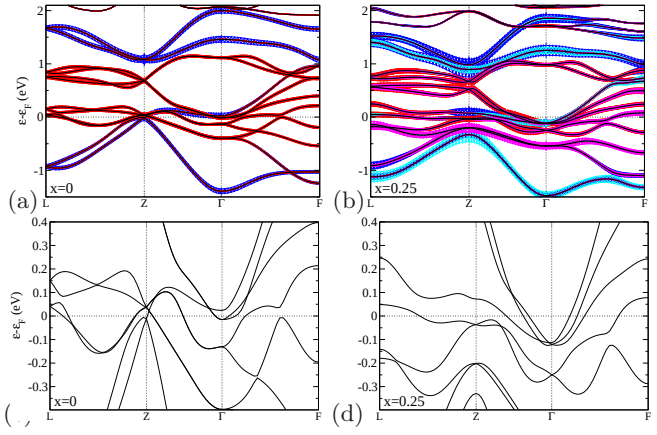

FIG. 2. Low-energy KS band structure for (a,c) undoped V_2O_3 and (b,d) Cr-doped with $x = 0.25$. (a,b) Color-resolved a_{1g} (blue) and e'_g (red) weight. The respective light colours (cyan/pink) refer to the corresponding Cr-based t_{2g} orbitals.

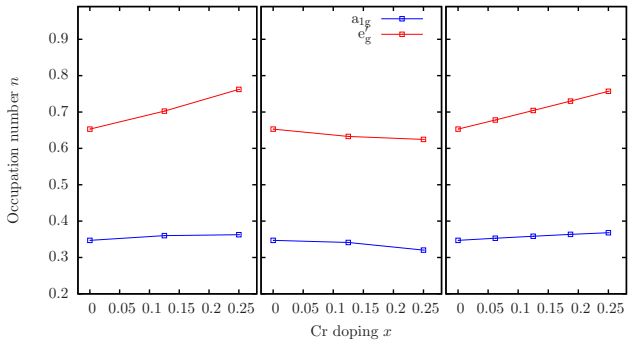

FIG. 3. (Color online) Average LDA occupation of the a_{1g} and e'_g orbitals with Cr doping. Left: from supercell calculations, averaged over Cr and V, middle: from supercell calculations, averaged over V only and right: within VCA.

site, while at Γ unoccupied electron-like bands barely touch ε_F. On the contrary for $V_{1.5}Cr_{0.5}O_2$ the multiple band crossings at Z have disappeared and the electron-like bands at Γ have now gained substantial occupation. It thus seems as if on the LDA level the Cr impurity resolves some delicate features of the V_2O_3 fermiology and transfers the electronic structure to a more stabilized regime. Interestingly, from Fig. 2(a,c) it becomes evident that the empty a_{1g}-like band along Z-Γ for x=0 crosses ε_F towards Γ for x=0.25. Note that in the latter doped case the occupied part of this band carries significant Cr-a_{1g} weight. On the local level the LDA crystal-field splitting between a_{1g} and e'_g on Cr turns out to be slightly larger than on V.

As shown in the occupation-number plot of Fig. 3, there is a polarization $\zeta = n_{e'_g}/n_{a_{1g}}$ of the e'_g orbital against the a_{1g} orbital already in stoichiometric V_2O_3 revealed by LDA calculation with eight transition-metal ions in the primitive cell. More interestingly, with Cr doping the average polarization ζ slightly increases. This however mainly happens due to the increased local ζ on the Cr ion. Fig. 3 shows that the polarization is nearly unchanged on the remaining V ions in the system with doping. Thus the additional electron due to Cr stays on its host ion and preferably occupies there the e'_g states in the LDA description. Note that the V occupation even seems to decrease slightly with Cr doping.

IV. EFFECT OF ELECTRONIC CORRELATIONS WITHIN DFT+DMFT

A. Isostructural effects

We now turn to an extended treatment of the electronic structure by including realistic electron correlation within the DFT+DMFT scope. To begin with, the structural parameters (including the LDA-relaxed Wyckoff positions) are not altered when turning to the advanced many-body investigation. This allows to clearly seperate electronic from structural influences of chromium doping.

The obtained k-integrated spectral function above the antiferromagnetic ordering temperature shown in Fig. 4a compares well to recent experimental data from photoemission spectroscopy by Mo *et al.*[26] In the stoichiometric case a low-energy resonance close to −0.3eV and a shallow lower Hubbard peak at around −1.5eV appears in the spectrum. Although our doping is much larger than in experiment, the qualitative feature due to Cr impurities, namely a surpression of the low-energy quasiparticle (QP) peak with spectral-weight transfer to deeper more negative energies, agrees well with experimental findings. Note that from our calculation a *sole* substitutional replacement of V by Cr at fixed crystal structure is not sufficient to render the system Mott-insulating. In other words, a Mott-insulating Cr-doped phase at the given LDA-optimized structural data cannot be stabilized without altering further parameters. An intricate interplay between electron doping *and* structural changes appears to trigger the metal-to-insulator transition in V_2O_3. Fig. 4(b,c) for the angle-resolved spectral data

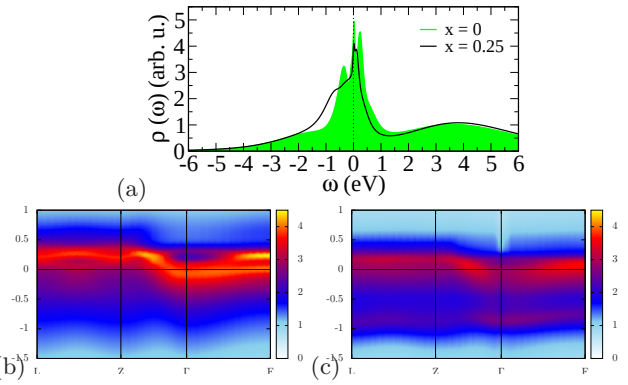

FIG. 4. (Color online) DFT+DMFT spectral data at T=166K. (a) k-integrated total spectral function. Low-energy angle-resolved spectral function along high-symmetry lines (b) without and (c) with x=0.25 Cr doping.

exhibits besides again the spectral weight transfer, band narrowing and substantial incoherency effects on the former noninteracting KS states well below room temperature. Interestingly especially in the undoped case the QP signature is stronger in the perpendicular-to-k_z plane through Γ than the one through Z. The resonance at low-energy is identified as a narrow QP state in the former plane. Also the renormalized band crossing along Z-Γ is a key feature of the angle-resolved data.

In order to investigate in more detail how explicit Cr doping influences the $n_{e'_g}/n_{a_{1g}}$ orbital polarization ζ in the correlated regime, we plot in Fig. 5 the respective t_{2g} occupations obtained within the DFT+DMFT supercell calculations. From averaging over all sites (including the Cr site) it is seen that a further increase of ζ compared to the LDA increase with doping occurs. The doping-induced polarization increase is mainly based on the the stronger e'_g occupation with Cr. Note that our polarization values turn out to be in good agreement with the numbers for Cr-doped V_2O_3 reported experimentally by Park *et al.*.[16] Although the occupation values averaged over *all* transition-metal sites are most appealing for an experimental comparison, the physical implications can more easily been studied if only vanadium sites are considered. Interestingly, the above-mentioned e'_g filling and the following increase of ζ is even stronger in that case. Hence this proves that electronic correlations are readily responsible for the additional (dopant) electron to leave its "home" on Cr. The role of the Cr-originating electron is thus not limited to a pure spectator, but directly affects also the local electronic characteristics of V . From the difference of the summed occupations, one can estimate the part of electrons leaving Cr to approximately 0.3-0.4. That the additional electron thus increases the polarization can be seen as a direct consequence of the spectrum, especially the strong bonding-antibonding character of a_{1g}, leaving few (but not zero, as mentioned above) spectral weight near the Fermi energy. Figure 5 shows furthermore that the orbital occupations (averaged again over all transition-metal sites) obtained from VCA calculations for doped V_2O_3 are in excellent agreement with the supercell-related results. It furthermore stresses the linear character of the polarization increase with Cr doping.

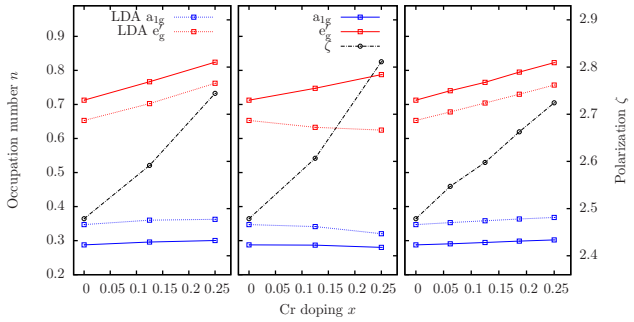

FIG. 5. (Color online) DFT+DMFT average occupation of the a_{1g} and e'_g orbitals and orbital polarization ζ. LDA data (dotted) repeated for comparison. Left: supercell calculations, averaged over Cr and V, middle: supercell calculations, averaged over V only, and right: VCA.

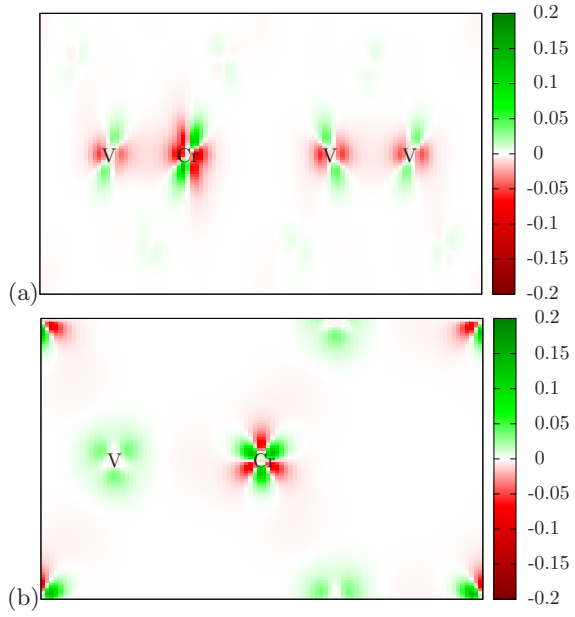

FIG. 6. (Color online) Difference $\Delta\rho$=$\rho_{\mathrm{DFT+DMFT}}-\rho_{\mathrm{LDA}}$ between correlated and LDA charge density for the doping level x=0.25. (a) Along (here horizontally aligned) c-axis, (b) within the honeycomb-lattice ab-plane of V_2O_3.

The correlation-induced local doping of V(e'_g) via Cr can also be visualized by plotting the charge-density difference $\Delta\rho$ between results from DFT+DMFT and LDA calculations (cf. Fig. 6). While along the c-axis $\Delta\rho$ dominantly exhibits the generic charge transfer within the t_{2g} manifold, the enhanced e'_g filling on V is obvious within the ab honeycomb plane of the corundum structure.

An intuitive understanding for the correlation-induced charge transfer from Cr to V is based on the increased local Coulomb energy introduced by the stronger filled t_{2g} of Cr compared to V. Nominally t_{2g} half-filled, Coulomb interactions on Cr give rise to a larger self-energy and increased repulsion energy. Reducing the charge inhomogenity via transferring part of the Cr electrons to V, leads to an overall energy lowering (partly through gain of kinetic energy).

B. Influence of the ratio $\frac{c}{a}$

Apart from the explicit Cr doping, another important ingredient for the exact behaviour of the orbital polarisation might be the ratio $\frac{c}{a}$ of the hexagonal crystallographic parameters. Since a small discontinuous jump thereof has been reported at the metal-insulator transition,[18,25] it is worth investigating the interplay of that ratio with explicit Cr doping. The value $\frac{c}{a}$∼2.82 in the metallic regime is large compared to other materials with

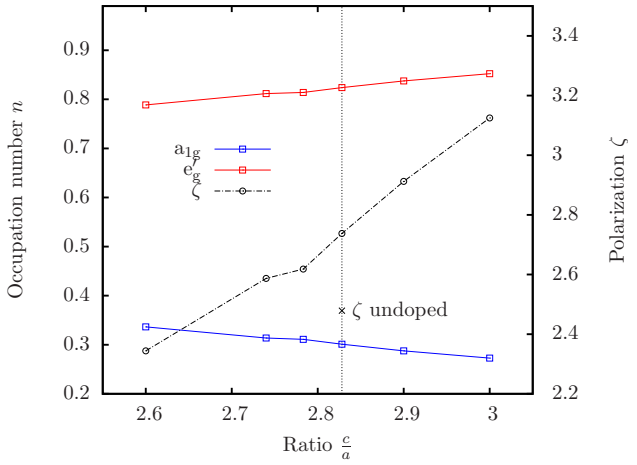

FIG. 7. (Color online) Occupation of the a_{1g} and e_g' orbitals and orbital polarization ζ with varying ratio $\frac{c}{a}$ at a doping of $x = 0.25$. The vertical dotted line marks the experimentally obtained value within the metallic phase used in the previous calculations.

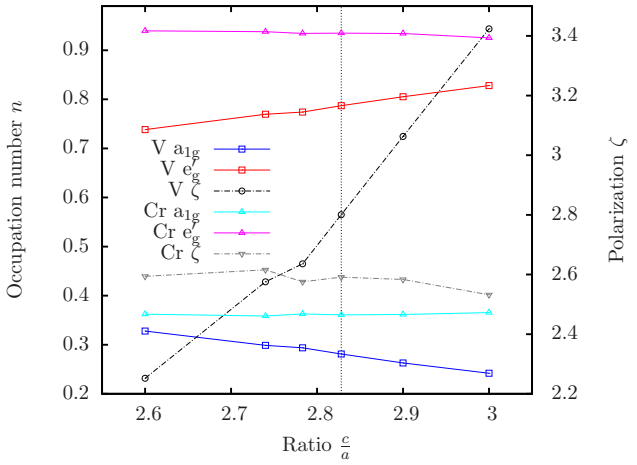

FIG. 8. (Color online) Vanadium and chromium resolved occupation numbers and ζ with varying ratio $\frac{c}{a}$ at a doping of $x = 0.25$. Vertical dotted line as in Fig. 7.

the same lattice structure,[25] and is slightly lowered to about 2.78 in the Mott-insulating phase. Here we derive results from supercell calculations with fixed unit-cell volume and LDA-relaxed Wyckoff positions for the case of rather large Cr doping (x=0.25). The overall evolution of the occupation numbers with $\frac{c}{a}$ ratio is displayed in Fig. 7. The decrease of the orbital polarization ζ with lower $\frac{c}{a}$ is the expected result. A more balanced value for the latter should render the transition-metal environment more isotropic and thus bring the orbital occupations closer together. Similar behaviour has also been found when doing the same calculation for the undoped system (not shown here). However, this does not imply that the increase of polarization due to explicit Cr doping can completely be reversed due to the change of the $\frac{c}{a}$ ratio. Through comparison to the polarization in the undoped case it is obvious that the doping-driven enhancement of ζ may qualitatively still be strong enough to overcome the reduction via a decreased $\frac{c}{a}$ ratio (see Fig. 7). As another observation, by studying the occupation numbers in an atomic-species-resolved way, shown in Fig. 8, it can be seen that the variation of ζ is completely related to the vanadium atoms. The chromium orbital occupations are essentially unaffected by any change of $\frac{c}{a}$. A possible reason for that is the initially higher crystal-field splitting of the respective Cr orbitals. Consequently, at least the Cr-orbital-related part of the doping-related polarization increase will persist when the $\frac{c}{a}$ ratio changes in the Mott-insulating phase.

The physical origin of the discontinuous jump of the $\frac{c}{a}$ ratio was previously shown to be primarily due to the increase of the unit-cell volume,[9] i. e. was part of the negative-pressure effect. However our calculations show that DFT+DMFT relaxed values of $\frac{c}{a}$ in the metallic Cr-doped material at *constant* unit-cell volume are found to be even higher than in the undoped case. Thus an *increased* unit-cell size in the doped regime would surely lead to an (overall) lowering of $\frac{c}{a}$, as also shown experimentally.[18] A complete quantitative first-principles account of the V_2O_3 MIT has therefore to address the delicate interplay between crystal-structure changes and Cr-doping in both the metallic and the insulating regime.

V. SUMMARY AND DISCUSSION

This work demonstrates that substitutional doping of V_2O_3 with Cr atoms (non-isovalent with V) has an sophisticated impact on the detailed correlated electronic structure that cannot be traced back to a pure (negative) pressure effect. Dispersion and filling of the QP bands (especially along k_z) change substantially by introducing Cr to the system. The orbital polarization between the relevant low-energy e_g' and a_{1g} states increases due to the electron doping. Notably correlation-induced charge transfers from Cr to V occur that are absent on the LDA level. This can explain why no occupation changes can be measured and calculated if only pressure is used to directly trigger the MIT. Thus including the true electron-doping physics does not require an increase of the effective crystal-field splitting of the *undoped* compound, as obtained when the MIT is modelled by an increase of the Hubbard U.[8] It has to be noted that the increase of orbital polarization displayed herein is nearly linear with the doping level. The experimentally observed discontinous jump of the polarization thus has to be explained by further non-continuous processes occuring at this fascinating metal-to-insulator transition, most surely through the intricate coupling to the lattice. Further correlated calculations with doping in the insulating regime are necessary to reveal more details on this matter. Moreover it is known from experiment that the dopant atoms in V_2O_3 are not homogeneously distributed in the crystal.[27] But

modellings thereof ask for much larger supercells with different impurity configurations, which at present is beyond the scope of practicable DFT+DMFT (and would also be extremely expensive already on the LDA level). It is nonetheless expected that such advanced modellings would mainly amplify the effects that are described in this work.

ACKNOWLEDGMENTS

We would like to thank M. Sandri and M. Fabrizio for helpful discussions. This work has been supported by the European Union, Seventh Framework Programme, under the project GO FAST, grant agreement no. 280555 and the DFG-FOR1346 program. Computations have been performed at the Juropa Cluster of the Jülich Supercomputing Centre (JSC) under project number hhh08.

[1] C. Castellani, C. R. Natoli, and J. Ranninger, Phys. Rev. B **18**, 4945 (1978)
[2] L. F. Mattheiss, J. Phys.: Condens. Matter **6**, 6477 (1994)
[3] S. Y. Ezhov, V. I. Anisimov, D. I. Khomskii, and G. A. Sawatzky, Phys. Rev. Lett. **83**, 4136 (1999)
[4] I. S. Elfimov, T. Saha-Dasgupta, and M. A. Korotin, Phys. Rev. B **68**, 113105 (2003)
[5] V. Eyert, U. Schwingenschlögl, and U. Eckern, Europhys. Lett. **70**, 782 (2005)
[6] K. Held, G. Keller, V. Eyert, D. Vollhardt, and V. I. Anisimov, Phys. Rev. Lett. **86**, 5345 (2001)
[7] G. Keller, K. Held, V. Eyert, D. Vollhardt, and V. I. Anisimov, Phys. Rev. B **70**, 205116 (2004)
[8] A. I. Poteryaev, J. M. Tomczak, S. Biermann, A. Georges, A. I. Lichtenstein, A. N. Rubtsov, T. Saha-Dasgupta, and O. K. Andersen, Phys. Rev. B **76**, 085127 (2007)
[9] D. Grieger, C. Piefke, O. E. Peil, and F. Lechermann, Phys. Rev. B **86**, 155121 (2012)
[10] M. Sandri, M. Capone, and M. Fabrizio, Phys. Rev. B **87**, 205108 (2013)
[11] Y. Guo, S. J. Clark, and J. Robertson, J. Chem. Phys. **140**, 054702 (2014)
[12] D. B. McWhan, J. B. Remeika, T. M. Rice, W. F. Brinkman, J. P. Maita, and A. Menth, Phys. Rev. Lett. **27**, 941 (1971)
[13] D. B. McWhan, A. Menth, J. B. Remeika, T. M. Rice, and W. F. Brinkman, Phys. Rev. B **7**, 1920 (1973)
[14] Y. Ding, C.-C. Chen, Q. Zeng, H.-S. Kim, M. J. Han, M. Balasubramanian, R. Gordon, F. Li, L. Bai, D. Popov, S. M. Heald, T. Gog, H.-k. Mao, and M. van Veenendaal, Phys. Rev. Lett. **112**, 056401 (2014)
[15] W. Bao, C. Broholm, S. A. Carter, T. F. Rosenbaum, G. Aeppli, S. F. Trevino, P. Metcalf, J. M. Honig, and J. Spalek, Phys. Rev. Lett. **71**, 766 (1993)
[16] J.-H. Park, L. H. Tjeng, A. Tanaka, J. W. Allen, C. T. Chen, P. Metcalf, J. M. Honig, F. M. F. de Groot, and G. A. Sawatzky, Phys. Rev. B **61**, 11506 (2000)
[17] F. Rodolakis, P. Hansmann, J.-P. Rueff, A. Toschi, M. W. Haverkort, G. Sangiovanni, A. Tanaka, T. Saha-Dasgupta, O. K. Andersen, K. Held, M. Sikora, I. Alliot, J.-P. Itié, F. Baudelet, P. Wzietek, P. Metcalf, and M. Marsi, Phys. Rev. Lett. **104**, 047401 (2010)
[18] F. Rodolakis, J.-P. Rueff, M. Sikora, I. Alliot, J.-P. Itié, F. Baudelet, S. Ravy, P. Wzietek, P. Hansmann, A. Toschi, M. W. Haverkort, G. Sangiovanni, K. Held, P. Metcalf, and M. Marsi, Phys. Rev. B **84**, 245113 (2011)
[19] B. Meyer, C. Elsässer, F. Lechermann, and M. Fähnle, *FORTRAN 90 Program for Mixed-Basis-Pseudopotential Calculations for Crystals*, Max-Planck-Institut für Metallforschung, Stuttgart (unpublished)
[20] P. Werner, A. Comanac, L. de' Medici, M. Troyer, and A. J. Millis, Phys. Rev. Lett. **97**, 076405 (2006)
[21] M. Ferrero and O. Parcollet, "TRIQS: a Toolbox for Research in Interacting Quantum Systems," `http://ipht.cea.fr/triqs`
[22] B. Amadon, F. Lechermann, A. Georges, F. Jollet, T. O. Wehling, and A. I. Lichtenstein, Phys. Rev. B **77**, 205112 (2008)
[23] V. I. Anisimov, D. E. Kondakov, A. V. Kozhevnikov, I. A. Nekrasov, Z. V. Pchelkina, J. W. Allen, S.-K. Mo, H.-D. Kim, P. Metcalf, S. Suga, A. Sekiyama, G. Keller, I. Leonov, X. Ren, and D. Vollhardt, Phys. Rev. B **71**, 125119 (2005)
[24] M. Karolak, T. O. Wehling, F. Lechermann, and A. I. Lichtenstein, J. Phys.: Condens. Matter **23**, 085601 (2011)
[25] P. D. Dernier, J. Phys. Chem. Solids **31**, 2569 (1970)
[26] S.-K. Mo, H.-D. Kim, J. D. Denlinger, J. W. Allen, J.-H. Park, A. Sekiyama, A. Yamasaki, S. Suga, Y. Saitoh, T. Muro, and P. Metcalf, Phys. Rev. B **74**, 165101 (2006)
[27] L. B. S. Lupi, B. Mansart, A. Perucchi, A. Barinov, P. Dudin, E. Papalazarou, F. Rodolakis, J.-P. Rueff, S. Ravy, D. Nicoletti, P. Postorino, P. Hansmann, N. Parragh, A. Toschi, T. Saha-Dasgupta, O. K. Andersen, G. Sangiovanni, K. Held, and M. Marsi, Nature Communications **1**, 105 (2010)